Report

Regulation of Mitotic Spindle Asymmetry by SUMO and the Spindle-Assembly Checkpoint in Yeast

Christian Leisner,[1,3] Daniel Kammerer,[2,3] Annina Denoth,[1,3] Mirjam Britschi,[1] Yves Barral,[1,*] and Dimitris Liakopoulos[2]
[1]Institute of Biochemistry
Department of Biology
Swiss Federal Institute of Technology (ETH Zurich)
Schafmattstrasse 18
8093 Zurich
Switzerland
[2]Biochemistry Center Heidelberg (BZH)
Heidelberg University
INF 328
69120 Heidelberg
Germany

Summary

During mitosis, the kinetochore microtubules capture and segregate chromosomes, and the astral microtubules position the spindle within the cell. Although the spindle is symmetric, proper positioning of the spindle in asymmetrically dividing cells generally correlates with the formation of morphologically and structurally distinct asters [1]. In budding yeast, the spindle-orientation proteins Kar9 and dynein decorate only one aster of the metaphase spindle and direct it toward the bud [2, 3]. The mechanisms controlling the distribution of Kar9 and dynein remain unclear. Here, we show that SUMO regulates astral-microtubule function in at least two ways. First, Kar9 was sumoylated in vivo. Sumoylation and Cdk1-dependent phosphorylation of Kar9 independently promoted Kar9 asymmetry on the spindle. Second, proper regulation of kinetochore function by SUMO was also required for Kar9 asymmetry. Indeed, activation of the spindle-assembly checkpoint (SAC) due to SUMO and kinetochore defects promoted symmetric redistribution of Kar9 in a Mad2-dependent manner. The control of Kar9 distribution by the SAC was independent of Kar9 sumoylation and phosphorylation. Together, our data reveal that three independent mechanisms contribute to Kar9 asymmetry: Cdk1-dependent phosphorylation, sumoylation, and SAC signaling. Hence, the two seemingly independent spindle domains, kinetochores and astral microtubules, function in a tightly coordinated fashion.

Results

Kar9 Is Sumoylated In Vivo

In former studies [4, 5], we noticed that Kar9 overexpression is lethal in cells lacking the septin-dependent kinase (SDK) Hsl1, but not in wild-type cells (unpublished data). Hoping to study this effect, we screened for *kar9* alleles that already showed toxicity upon overexpression in wild-type cells (Figure 1A; also see Supplemental Experimental Procedures, available online). Four alleles were identified. One mutation substituted

*Correspondence: yves.barral@bc.biol.ethz.ch
[3]These authors contributed equally to this work

K333 to E, and a second mutation substituted T344 to A. Remarkably, the remaining two mutations replaced conserved lysines with arginines (K301 and K381), indicating that these mutations did not simply change charges on the protein. Importantly, the alleles that combined the lysine mutations (Kar9-3K, along with Kar9-3R and Kar9-4R; see below) were toxic neither when overexpressed nor at endogenous levels (Figure 1A and Figure S1A). This study focuses on the observation that the mutation K301R falls in a predicted sumoylation site (Figure 1B) [6–8], which suggests that these mutations might identify sumoylation sites on Kar9.

To investigate whether Kar9 is sumoylated in vivo, we transiently overexpressed N-terminally His-tagged Smt3 from the *CUP1* promoter in yeast cells in which Kar9, expressed at endogenous levels, was C terminally TAP tagged. [HIS]SUMO conjugates were purified from extracts under denaturing conditions with a nickel column [9], and then western-blot analysis with antibodies against Kar9-TAP was performed. Under these conditions, Kar9-TAP was pulled down even in the absence of SUMO induction, as previously reported for other proteins [10]. Upon [HIS]SUMO induction, a second immunoreactive band with reduced electrophoretic mobility appeared (Figure 1D). This band ran approximately 15 kDa higher than Kar9-TAP, consistent with modification of Kar9 by a single SUMO moiety. The temperature-sensitive mutation *ulp1-333* in the SUMO protease gene *ULP1* causes numerous SUMO conjugates to accumulate [11]. It also caused the proportion of the slow-migrating Kar9-TAP isoforms to strongly increase (Figure 1D). Furthermore, cells lacking the two redundant sumoylation E3 enzymes Siz1 and Siz2 [12, 13] failed to produce slow-migrating isoforms of Kar9 (Figure 1G). We concluded that Kar9 was indeed sumoylated in vivo in a Siz1- and Siz2-dependent manner and that its desumoylation depended on Ulp1.

Next, we asked whether the lysines identified in our screen were sumoylation sites. Mutation of each lysine individually or in pairs did not significantly affect Kar9 sumoylation levels in vivo (Figure 1E and the K301R K333E double mutant Kar9-RE in Figure 1F). However, when all three identified mutations were combined (Kar9-2RE), and when all three lysines were mutated to arginines (Kar9-3R), sumoylation was significantly reduced, although not fully abolished (Figures 1F and 1G). Interestingly, Kar9 contains two additional matches to a weaker sumoylation consensus site at lysines K76 and K529. Although changing either of these lysines individually to arginine had no effect on Kar9 sumoylation levels (Figure 1E and data not shown), when the K529R mutation was introduced into Kar9-3R to form Kar9-4R, no modified Kar9 was detectable (Figure 1G), indicating that all main sumoylation sites had been mutated. We concluded that K381, K301, K333, and K529 are used for sumoylation in vivo.

Sumoylation Regulates Kar9 Asymmetry and Spindle Positioning

During metaphase, Kar9 predominantly decorates the astral microtubules emanating from one spindle pole body (SPB) and guides them toward the bud [2, 3, 14]. This leads to pulling of the spindle toward the bud and to its alignment with the mother-bud axis. Hence, the distance (d) between the spindle
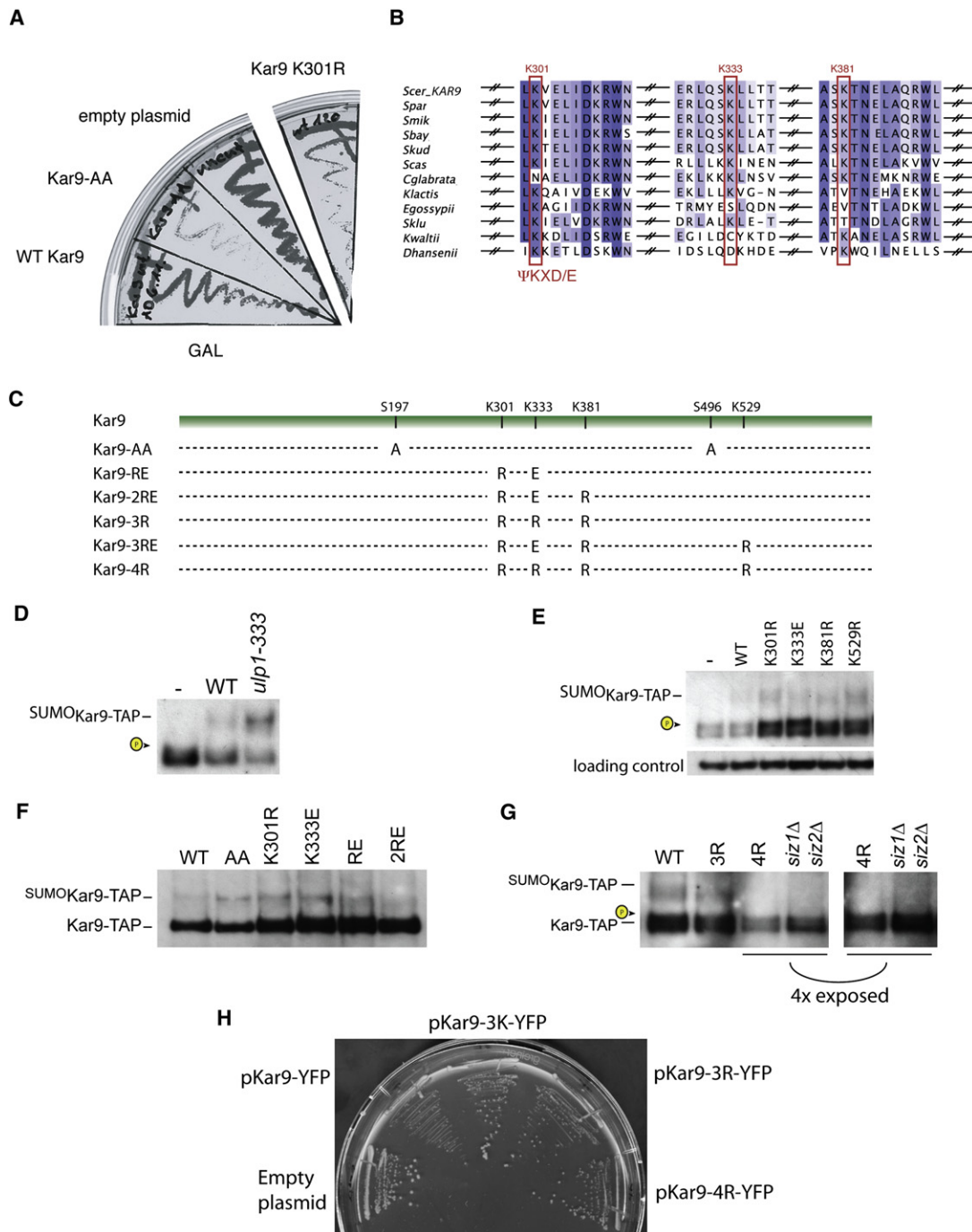
Figure 1. Conserved Lysines in Kar9 Are Modified by SUMO

(A) Growth test of strains overexpressing different *KAR9* alleles obtained from random mutagenesis. Kar9-K301R overexpression reduces growth more than overexpression of WT Kar9 and less than overexpression of Kar9-AA. Kar9-K333E, Kar9-K381R, and T344A were identified as showing a similar growth phenotype.

(B) Conservation of the identified lysines in Kar9. K301 is part of the only ΨKXD/E consensus site for sumoylation in Kar9 (Clustal X alignment).

(C) Overview of Kar9 variants containing multiple missense mutations.

(D) Purification of denatured [His]SUMO-Kar9-TAP conjugates by nickel-affinity chromatography, from cells expressing [His]SUMO under the copper-inducible *CUP1p* promoter. [His]SUMO conjugates were subjected to western blotting against TAP. Kar9-TAP sticks to the nickel beads under these conditions, but the modified form appeared only after [His]SUMO induction. [His]SUMO pull-downs were performed in WT cells and *ulp1-333* cells. All pull-downs were performed at RT except for those in *ulp1-333*, which were made at 37°C. "-" represents the uninduced negative control.

(E) Purification of [His]SUMO Kar9-TAP single-lysine variants isolated as described above. K333E was originally isolated in the overexpression screen.

(F) Purification of [His]SUMO Kar9-TAP single-, double-, and triple-lysine variants isolated as described above. The double mutant RE (K301R K333E) did not show a significant decrease in sumoylation. However, additional mutation of K381 to R (2RE) reduced the level of sumoylation.

(G) Purification of [His]SUMO Kar9-TAP triple and quadruple mutants (3R and 4R) and WT Kar9-TAP in *siz1Δsiz2Δ* cells. All pull-downs were performed at RT.
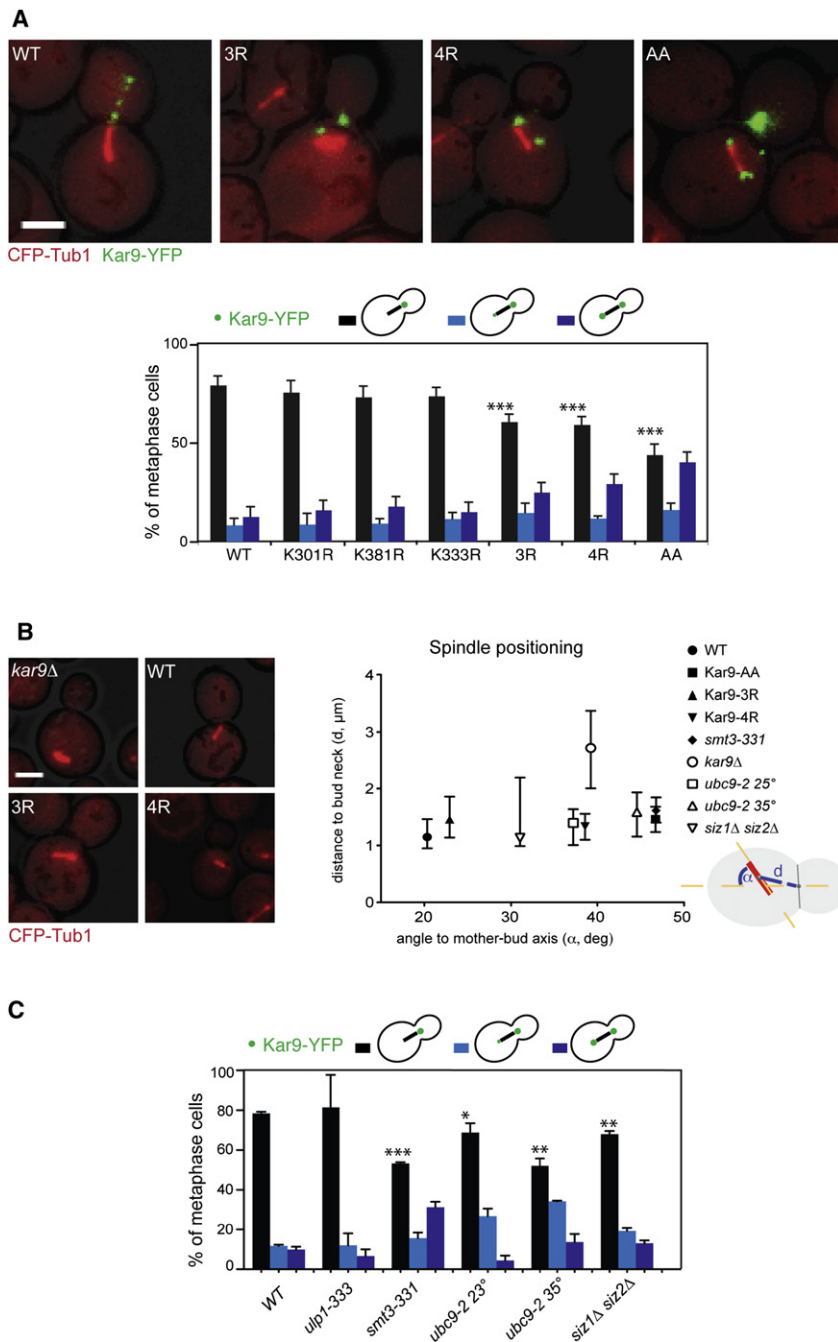
A

Figure 2. Sumoylation Is Required for Kar9 Asymmetry

(A) Images show maximum projections of representative cells expressing CFP-Tub1 and Kar9-YFP variants (the scale bar represents 2 μm). The graph shows quantification of Kar9 localization in metaphase cells expressing Kar9-YFP, Kar9-K301R-YFP, Kar9-K381R-YFP, Kar9-K333R-YFP, Kar9-3R-YFP, Kar9-4R-YFP, and Kar9-AA-YFP with time-lapse fluorescence microscopy. Cells with Kar9-YFP signal were divided into three categories: strong asymmetry (Kar9 localizing to only one SPB and astral microtubules), weak asymmetry (Kar9 localizing to both poles but showing less than 50% fluorescence intensity on one pole), and symmetry. Statistical significance was determined by Student's t test. ***p < 0.001 with n = 4 independent experiments (minimum 200 cells in total).

(B) Images of maximum projections of cells expressing CFP-Tub1 (the scale bar represents 2 μm). Spindle positioning in cells expressing C-terminally YFP-tagged Kar9, Kar9-AA, −3R, and −4R compared to *kar9Δ* cells. Spindle positioning was quantified by measuring the distance from the center of the spindle to center of the bud neck (d) and the angle between the spindle axis and the mother-bud axis (α). Spindle positioning was quantified in WT, *smt3-331*, *ubc9-2* at 25°C, *ubc9-2* at 35°C, *siz1Δsiz2Δ*, and *kar9Δ* cells, as well as in cells expressing Kar9-AA, Kar9-3R, and Kar9-4R as the only versions of Kar9. The analysis was performed in movies of 10 frames and for a minimum of 270 frames (27 cells) per strain. The graphs show the median values and the 25–75 percentile range.

(C) Localization of Kar9-YFP in wild-type cells and the mutants, *ulp1-333* at 37°C, *smt3-331* at 30°C, *ubc9-2* at 23°C, *ubc9-2* at 35°C, and *siz1Δ siz2Δ* at RT. Quantifications were made as in Figure 2A. *p < 0.05, **p < 0.01, ***p < 0.001.

B

C

To investigate the role of sumoylation in Kar9 regulation, we imaged Kar9-3R-YFP and Kar9-4R-YFP in cells expressing CFP-Tubulin. These alleles replaced endogenous Kar9, allowing us to characterize the effect of these point mutations on spindle positioning. Preventing Kar9 sumoylation did not affect spindle migration to the bud neck (Figure 2B). However, both Kar9-3R-YFP and Kar9-4R-YFP localized more symmetrically on metaphase spindles than Kar9-YFP did (symmetry: 39% ± 4%, n = 4; 41% ± 4%, n = 4; and 21%, respectively, p < 0.001; Figure 2A). Accordingly, these alleles caused the mean value for α to increase (Figure 2B), i.e., compromised spindle alignment with the mother-bud axis. Thus, Kar9 sumoylation inhibited Kar9 accumulation on the mother-directed SPB and emanating astral microtubules.

To further investigate SUMO's role in Kar9 localization and function, we monitored spindle position and Kar9 distribution in cells defective in the sumoylation machinery (sumoylation reviewed in [17]). Similar to cells expressing Kar9-3R or

and the bud neck (Figure 2B) and the angle (α) between the spindle and the mother-bud axis remain low. When Kar9 is absent, astral microtubules do not orient, both migration and alignment of the metaphase spindle fail [15], and the values for d and α both remain high (Figure 2B). Conversely, the non-phosphorylatable protein Kar9-AA decorates the microtubules emanating from both poles in a large fraction of the cells (56% ± 5%, n = 4 versus 21% ± 5%, n = 4 for wild-type Kar9, p < 0.001; Figure 2A) [1, 16]. Although the spindle migrates properly to the bud neck, both SPBs are pulled toward the bud. Thus, although d decreases as in the wild-type, the spindle fails to stably align and α is high (Figure 2B).

(H) Growth upon overexpression of WT Kar9, Kar9-3K, Kar9-3R, and Kar9-4R. Cells containing a 2μ plasmid with no *KAR9* gene or with the three *kar9* alleles mentioned above under control of a *GAL1* promoter were grown on −Leu GAL plates. The colony sizes for each strain reflect the growth rate.
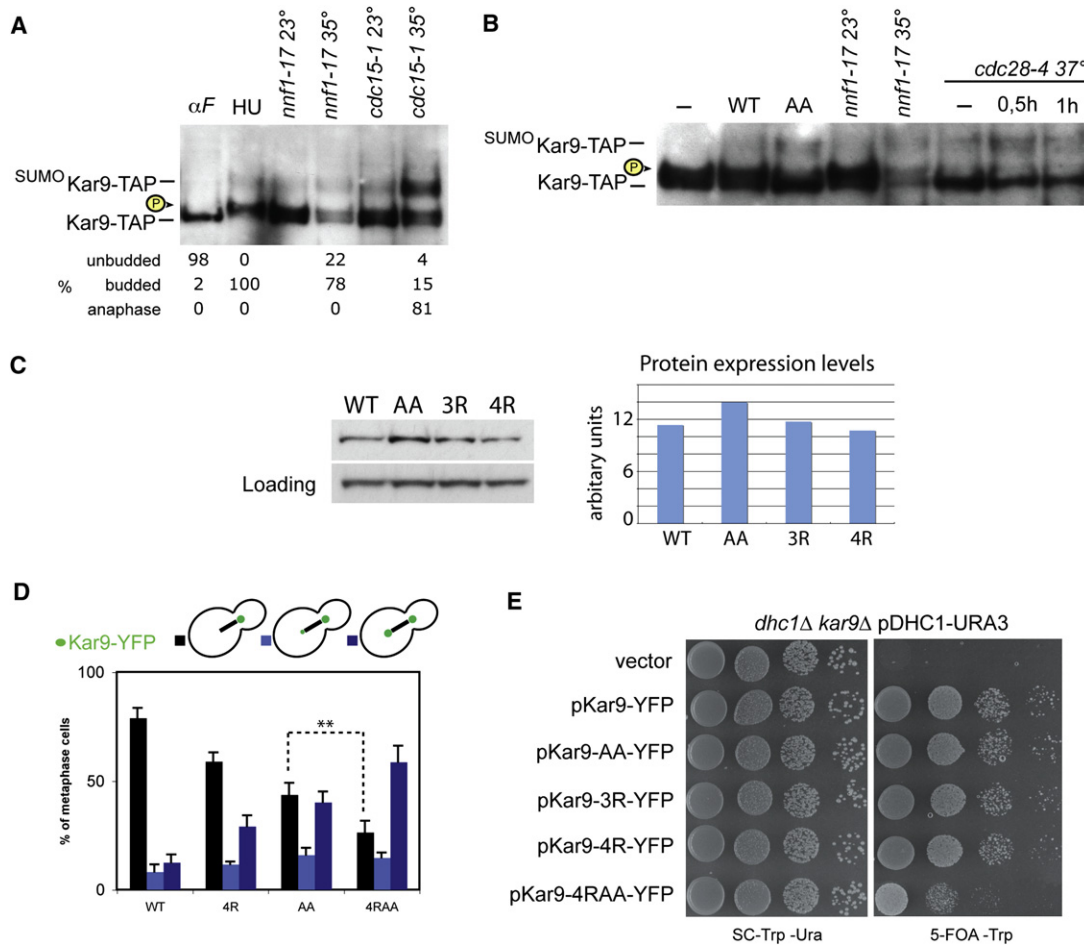
Figure 3. Sumoylation and Phosphorylation Regulate Kar9 Asymmetry Independently

(A) Cell-cycle dependence of Kar9 sumoylation. SUMO pull-down and Kar9-TAP detection in cells arrested in G1 (α-factor), metaphase (HU: hydroxyurea), metaphase (nnf1-17), and anaphase (cdc15-1). His-SUMO Kar9-TAP pull-downs were made as described in Figure 1. The quantifying budding index monitored the cell-cycle stage for each condition.

(B) Estimating Kar9 sumoylation and phosphorylation by SUMO pull-downs in Kar9 phosphomutants and upon SAC activation. Sumoylation was monitored in Kar9-AA expressing cells and in cells expressing cdc28-4 at 37°C. In addition, we monitored Kar9 sumoylation in nnf1-17 cells at restrictive temperature (35°C). His-SUMO Kar9-TAP pull-downs were made as described in Figure 1.

(C) Western-blot analysis of C-terminally TAP tagged Kar9, Kar9-AA, Kar9-3R, and Kar9-4R. Lysates were separated on a high-percentage gel to get a sharp band, and band intensities were quantified with densitometry (graph).

(D) Kar9 localization in cells expressing C-terminally YFP-tagged Kar9, Kar9-AA, −4R, and −4RAA. Quantifications were made as in Figure 2. **p < 0.01 with n = 4 independent experiments (minimum 200 cells in total).

(E) Synthetic lethality between dhc1Δ and Kar9 mutants. C-terminally YFP-tagged Kar9, Kar9-AA, −3R, −4R, and −4RAA were expressed in dhc1Δ kar9Δ pDHC1:URA3 cells. Growth was monitored by spot test on −Trp −Ura plates (pDHC1:URA3 present) and on 5-FOA −Trp (no pDHC1:URA3).

Kar9-4R, the siz1Δ siz2Δ mutant cells showed increased Kar9 symmetry (Figure 2C), and spindles were misaligned yet migrated properly to the bud neck (Figure 2B). In contrast, the ulp1-333 mutant cells showed no significant defects in Kar9 distribution (Figure 2C). Thus, Kar9 asymmetry required SUMO conjugation but no sumoylation-desumoylation cycle.

The smt3-331 [18] and ubc9-2 temperature-sensitive mutations in the sumo protein and the sumoylation E2 enzyme Ubc9 increased Kar9 symmetry to 47% ± 1%, n = 3 (30°C, 1 hr) and to 48% ± 4%, n = 3 (35°C, 2 hr; Figure 2C), respectively, which was more than the unsumoylated protein Kar9-4R-YFP (41% ± 4%, n = 4; Figure 2A). Consistently, they caused stronger spindle misalignment than Kar9-4R (Figure 2B). Thus, cells with overall sumoylation defects displayed more severe defects in Kar9 function than cells with nonmodified Kar9. We concluded that the failure of sumoylating Kar9 is not the sole cause of the spindle-positioning phenotypes observed in the smt3-331 and ubc9-2 mutant cells.

Sumoylation and Phosphorylation Control Kar9 Asymmetry Independently

Because Kar9 asymmetry is a mitotic event, we investigated whether the sumoylation of Kar9 varied during the cell cycle, using pull-downs as above. Kar9 was hardly sumoylated in G1-arrested cells (alpha-factor-arrested cells; Figure 3A). Hydroxyurea (HU) arrests yeast cells with incompletely replicated DNA, a well-formed metaphase spindle, and high levels of securin (Pds1) and Cdc28/Clb2 kinase [19, 20]. In these cells, Kar9 was sumoylated (Figure 3A). In cells arrested at the spindle-assembly checkpoint (SAC) because of nocodazole treatment or inactivation of the temperature-sensitive kinetochore protein Nnf1-17, expression of tagged-SUMO was highly toxic.
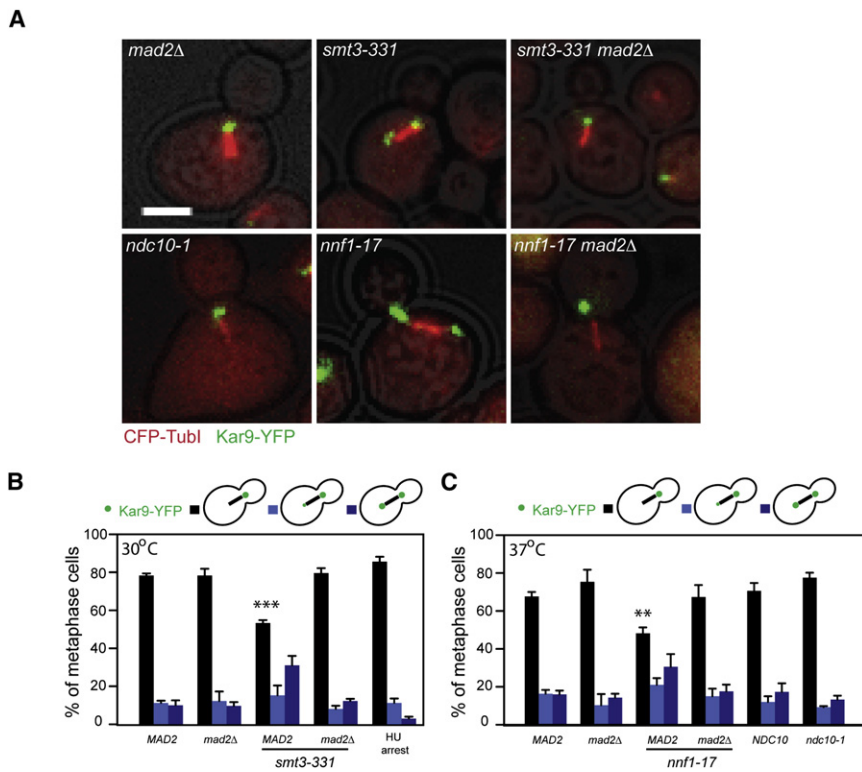
A

CFP-TubI   Kar9-YFP

B

C

Figure 4. Activation of the Spindle-Assembly Checkpoint Leads to Symmetrically Distributed Kar9 in *smt3-331*

(A) Images of maximum projections of representative metaphase cells expressing CFP-Tub1 and Kar9-YFP (the scale bar represents 2 μm).

(B) Quantification of Kar9 asymmetry in WT, *mad2Δ*, *smt3-331*, and *smt3-331 mad2Δ* cells in metaphase. Cells were grown at RT and shifted to 30°C for 60 min. ***p < 0.001 with n = 3 independent experiments and standard deviations shown as error bars (minimum 150 cells in total).

(C) Quantification of Kar9 asymmetry in WT, *mad2Δ*, *nnf1-17*, and *nnf1-17 mad2Δ* cells (grown at RT and shifted to 37°C for 90 min) and in WT and *ndc10-1* cells (alpha factor arrested and released at 37°C for 2–3 hr). **p < 0.01 with n = 3 independent experiments and standard deviations shown as error bars (minimum 150 cells in total).

In these cells, the amount of free Kar9 was reduced (Figures 3A and 3B). However, Kar9 sumoylation levels were comparable with those of HU-treated cells. Sumoylation was increased in cells arrested in anaphase because of the *cdc15-1* mutation (Figure 3A). Thus, Kar9 sumoylation correlated with spindle formation and persisted until the end of mitosis.

Cdk1-dependent phosphorylation of Kar9 also varies throughout the cell cycle to reach its highest level during S phase/metaphase [2, 16] (Figure 3A). Therefore, we investigated the interdependency between sumoylation and phosphorylation. In pull-down experiments, nonphosphorylatable Kar9, Kar9-AA, and Kar9 expressed in *cdc28-4* mutant cells that lacked Cdk1 activity were at least as efficiently sumoylated as wild-type Kar9 from wild-type cells (Figure 3B; see also Figure 1F). Conversely, the nonsumoylated variants Kar9-3R-TAP and Kar9-4R-TAP were as efficiently phosphorylated in wild-type cells as wild-type Kar9 (Figure 1G). The steady-state levels of the Kar9 variants did not vary much either (Figure 3C). Only the Kar9-AA level was somewhat elevated, although still comparable to wild-type (Figure 3C). Consistent with Kar9 phosphorylation and sumoylation occurring independently of each other, the Kar9-4RAA-YFP allele, which altogether lacked the main sumoylation and Cdk1 phosphorylation sites, localized much more symmetrically than that of either Kar9-4R-YFP or Kar9-AA-YFP (Figure 3D) and showed a stronger synthetic interaction than any of the single mutants (Figure 3E). Together, our data established that sumoylation and phosphorylation contributed independently to Kar9 asymmetry.

The Spindle-Assembly Checkpoint Impinges on Kar9 Localization

Because the phenotypes of the *smt3-331* and *ubc9-2* mutant cells were more severe than that caused by the nonsumoylated protein Kar9-4R, we investigated whether SUMO also affects Kar9 function through indirect processes. As previously reported [21], and consistent with many kinetochore proteins being sumoylated in vivo [22], we observed that *smt3-331 CFP-TUB1* mutant cells formed misshapen spindles (data not shown). Furthermore, cells with kinetochore defects sometimes show spindle-localization defects similar to those of the *smt3-331* mutant cells [23]. Thus, we wondered whether Kar9 distribution is linked to kinetochore function. We monitored Kar9 distribution in cells carrying temperature-sensitive alleles in the kinetochore genes *NDC10* and *NNF1*. At 37°C, the *ndc10-1* allele causes kinetochore dissociation from DNA and abrogates the SAC [24]. In these cells, Kar9-YFP localized as in wild-type cells (Kar9 symmetry: 23% ± 3%, n = 3 compared to 29% ± 4%, n = 3 in wild-type at 37°C; Figures 4A and 4C). At 37°C, the *nnf1-17* mutation impairs kinetochore-microtubule attachment, and the cells arrest at the SAC [25]. In these cells, Kar9-YFP distribution was much more symmetric (symmetry = 52% ± 3%, n = 3, p < 0.01 compared to wild-type; Figures 4A and 4C). Thus, in SAC-arrested cells, Kar9 distribution was quite symmetric, similar to *smt3-331* cells (Figures 4A and 4B).

Accordingly, the symmetry of Kar9 distribution in the *nnf1-17* mutant cells depended on SAC activation. Indeed, inactivation of the SAC effector gene *MAD2* [26] restored Kar9 asymmetry in the *nnf1-17* mutant cells grown at 37°C (Kar9 symmetry: 33% ± 6%, n = 3; Figures 4A and 4C). To test whether the effect of SAC activation reflected a specific role of the SAC in inhibiting Kar9 asymmetry or a general effect of cell-cycle arrest on Kar9 distribution, we took advantage of the fact that HU treatment and SAC activation lead to very similar cell-cycle-arrest phenotypes in yeast. In budding yeast, DNA replication and spindle assembly are concomitant, and both SAC activation and the DNA-replication checkpoint delay anaphase by preventing the degradation of the separase inhibitor securin ([19, 20] and reviewed in [27]). Whereas the SAC achieves this through inhibition of APC/Cdc20 by Mad2, the DNA-replication checkpoint promotes securin phosphorylation and stabilization directly. In contrast to SAC-arrested cells, HU-treated cells showed no increase in Kar9 symmetry (symmetry = 14% ± 2%, n = 3; Figure 4B). Thus, the impact of SAC activation on Kar9 distribution was not a mere

consequence of cell-cycle arrest. It was not due to a lack of Kar9 phosphorylation or sumoylation either: Kar9 was highly phosphorylated in nocodazole-treated cells, and in the *nnf1-17* cells shifted to the restrictive temperature for 3 hr, Kar9 phosphorylation and sumoylation levels were not affected (Figures 3A and 3B). Therefore, we concluded that SAC activation impinges on Kar9 distribution independently of phosphorylation and SUMO modification.

On the basis of these data, we next wondered whether the enhanced level of Kar9 symmetry observed in the *smt3-331* cells could be due to SAC activation in these cells. Supporting this interpretation, Kar9 asymmetry was fully restored in *mad2Δ smt3-331* cells compared to the *smt3-331* single-mutant cells (after 1 hr at 30°C, Kar9 symmetry was 20% ± 3%, n = 3 and 47% ± 1%, n = 3, respectively; Figures 4A and 4B). Thus, SUMO affects Kar9 distribution both directly through Kar9 modification and indirectly through its role in spindle assembly.

Discussion

Together, our study establishes that Kar9 is sumoylated in vivo mainly on four lysines (K301, K333, K381, and K529). Simultaneous mutation of these residues strongly impaired conjugation of SUMO onto the protein and proper Kar9 distribution. Furthermore, in cells lacking the two redundant SUMO ligases Siz1 and Siz2, Kar9 sumoylation was undetectable, Kar9 localized more symmetrically, and spindle alignment with the mother-bud axis was affected. Therefore, similar to its role in the regulation of microtubule-kinetochore attachment [22], SUMO regulates astral microtubules through modification of at least the plus-end-associated protein Kar9.

Sumoylation might prime Kar9 for subsequent ubiquitination and removal from the mother-bound pole through degradation. It might also control the multimerization of Kar9, its accessibility to other regulators, or its association with the microtubule-associated proteins Bim1, Bik1, and Stu2 [16, 28–31]. We favor this last option. Indeed, Kar9-3R and Kar9-4R variants are expressed at similar levels as wild-type Kar9, indicating that degradation does not play a major role in its regulation. Similarly, our data exclude the possibility that sumoylation controls the accessibility of Kar9 to Cdk1: Kar9 sumoylation and phosphorylation were not interdependent. In vitro sumoylation and binding assays will be required to address how SUMO regulates Kar9 distribution.

Remarkably, the *smt3-331* mutation affected Kar9 distribution mainly through the SAC. In the *smt3-331* mutant cells, SAC inactivation should have restored Kar9 asymmetry only to the levels observed with Kar9-4R. Why this was not observed is unclear. Possibly, sumoylation might be more rapidly depleted in the nucleus because many of the processes requiring SUMO appear to take place in that organelle.

Together, our data reveal the regulatory complexity underlying spindle asymmetry. At least three regulatory pathways control Kar9 distribution. As already reported, direct phosphorylation of Kar9 by Cdk1 reduces its affinity for microtubule-associated proteins such as Bim1 and Stu2 [2, 31]. However, preventing Cdk1-dependent phosphorylation of Kar9 only partially abrogates Kar9 asymmetry [2, 31], and the importance of this regulatory pathway might be variable between genetic backgrounds [32]. Here, we show that at least two additional pathways contribute to Kar9 regulation, namely sumoylation and the SAC. The fact that these two pathways are distinct from each other and from Cdk1-dependent regulation is evidenced by several converging observations. Most

conclusively, combining sumoylation- and phosphorylation-site mutations in Kar9-4RAA abrogates the asymmetric distribution of the protein more extensively than the 4R and AA mutations separately. Thus, sumoylation and phosphorylation act independently on Kar9. Furthermore, SAC activation does not interfere with Kar9 sumoylation and phosphorylation, indicating that the SAC downregulates a third pathway. Thus, our data are consistent with sumoylation, phosphorylation, and a third independent pathway acting in additive manners to robustly control Kar9 distribution. It will be important to identify the molecular mechanisms of the third pathway and to show how these pathways are regulated and how they crosstalk with one another to promote spindle asymmetry.

The functional significance of Kar9 regulation by the SAC is unclear. Interestingly, however, Kar9 symmetry upon SAC activation caused spindle movements and rotation that are reminiscent of the nuclear oscillations observed during meiosis in *Schizosaccharomyces pombe*. These dynein-dependent movements promote chromosome pairing in early meiosis [33, 34]. Similarly, the nuclear movements observed in the presence of kinetochore defects and due to SAC activation may facilitate kinetochore capture and the correction of spindle defects. Together, our observations indicate that kinetochore and astral microtubules form a much more integrated and coordinated system than previously anticipated.

References

1. Kusch, J., Liakopoulos, D., and Barral, Y. (2003). Spindle asymmetry: A compass for the cell. Trends Cell Biol. *13*, 562–569.
2. Liakopoulos, D., Kusch, J., Grava, S., Vogel, J., and Barral, Y. (2003). Asymmetric loading of Kar9 onto spindle poles and microtubules ensures proper spindle alignment. Cell *112*, 561–574.
3. Maekawa, H., Usui, T., Knop, M., and Schiebel, E. (2003). Yeast Cdk1 translocates to the plus end of cytoplasmic microtubules to regulate bud cortex interactions. EMBO J. *22*, 438–449.
4. Grava, S., Schaerer, F., Faty, M., Philippsen, P., and Barral, Y. (2006). Asymmetric recruitment of dynein to spindle poles and microtubules promotes proper spindle orientation in yeast. Dev. Cell *10*, 425–439.
5. Kusch, J., Meyer, A., Snyder, M.P., and Barral, Y. (2002). Microtubule capture by the cleavage apparatus is required for proper spindle positioning in yeast. Genes Dev. *16*, 1627–1639.
6. Rodriguez, M.S., Dargemont, C., and Hay, R.T. (2001). SUMO-1 conjugation in vivo requires both a consensus modification motif and nuclear targeting. J. Biol. Chem. *276*, 12654–12659.
7. Sampson, D.A., Wang, M., and Matunis, M.J. (2001). The small ubiquitin-like modifier-1 (SUMO-1) consensus sequence mediates Ubc9 binding

and is essential for SUMO-1 modification. J. Biol. Chem. *276*, 21664–21669.

8. Johnson, E.S., and Blobel, G. (1999). Cell cycle-regulated attachment of the ubiquitin-related protein SUMO to the yeast septins. J. Cell Biol. *147*, 981–994.

9. Sacher, M., Pfander, B., and Jentsch, S. (2005). Identification of SUMO-protein conjugates. Methods Enzymol. *399*, 392–404.

10. Panse, V.G., Hardeland, U., Werner, T., Kuster, B., and Hurt, E. (2004). A proteome-wide approach identifies sumoylated substrate proteins in yeast. J. Biol. Chem. *279*, 41346–41351.

11. Li, S.J., and Hochstrasser, M. (1999). A new protease required for cell-cycle progression in yeast. Nature *398*, 246–251.

12. Takahashi, Y., Kahyo, T., Toh, E.A., Yasuda, H., and Kikuchi, Y. (2001). Yeast Ull1/Siz1 is a novel SUMO1/Smt3 ligase for septin components and functions as an adaptor between conjugating enzyme and substrates. J. Biol. Chem. *276*, 48973–48977.

13. Johnson, E.S., and Gupta, A.A. (2001). An E3-like factor that promotes SUMO conjugation to the yeast septins. Cell *106*, 735–744.

14. Hwang, E., Kusch, J., Barral, Y., and Huffaker, T.C. (2003). Spindle orientation in Saccharomyces cerevisiae depends on the transport of microtubule ends along polarized actin cables. J. Cell Biol. *161*, 483–488.

15. Miller, R.K., and Rose, M.D. (1998). Kar9p is a novel cortical protein required for cytoplasmic microtubule orientation in yeast. J. Cell Biol. *140*, 377–390.

16. Moore, J.K., D'Silva, S., and Miller, R.K. (2006). The CLIP-170 homologue Bik1p promotes the phosphorylation and asymmetric localization of Kar9p. Mol. Biol. Cell *17*, 178–191.

17. Geiss-Friedlander, R., and Melchior, F. (2007). Concepts in sumoylation: A decade on. Nat. Rev. Mol. Cell Biol. *8*, 947–956.

18. Mahajan, R., Delphin, C., Guan, T., Gerace, L., and Melchior, F. (1997). A small ubiquitin-related polypeptide involved in targeting RanGAP1 to nuclear pore complex protein RanBP2. Cell *88*, 97–107.

19. Agarwal, R., Tang, Z., Yu, H., and Cohen-Fix, O. (2003). Two distinct pathways for inhibiting pds1 ubiquitination in response to DNA damage. J. Biol. Chem. *278*, 45027–45033.

20. Bachant, J., Jessen, S.R., Kavanaugh, S.E., and Fielding, C.S. (2005). The yeast S phase checkpoint enables replicating chromosomes to bi-orient and restrain spindle extension during S phase distress. J. Cell Biol. *168*, 999–1012.

21. Biggins, S., Bhalla, N., Chang, A., Smith, D.L., and Murray, A.W. (2001). Genes involved in sister chromatid separation and segregation in the budding yeast Saccharomyces cerevisiae. Genetics *159*, 453–470.

22. Montpetit, B., Hazbun, T.R., Fields, S., and Hieter, P. (2006). Sumoylation of the budding yeast kinetochore protein Ndc10 is required for Ndc10 spindle localization and regulation of anaphase spindle elongation. J. Cell Biol. *174*, 653–663.

23. Shan, X., Xue, Z., Euskirchen, G., and Melese, T. (1997). NNF1 is an essential yeast gene required for proper spindle orientation, nucleolar and nuclear envelope structure and mRNA export. J. Cell Sci. *110*, 1615–1624.

24. Fraschini, R., Beretta, A., Lucchini, G., and Piatti, S. (2001). Role of the kinetochore protein Ndc10 in mitotic checkpoint activation in Saccharomyces cerevisiae. Mol. Genet. Genomics *266*, 115–125.

25. Euskirchen, G.M. (2002). Nnf1p, Dsn1p, Mtw1p, and Nsl1p: A new group of proteins important for chromosome segregation in Saccharomyces cerevisiae. Eukaryot. Cell *1*, 229–240.

26. Chen, R.H., Brady, D.M., Smith, D., Murray, A.W., and Hardwick, K.G. (1999). The spindle checkpoint of budding yeast depends on a tight complex between the Mad1 and Mad2 proteins. Mol. Biol. Cell *10*, 2607–2618.

27. Peters, J.M. (2006). The anaphase promoting complex/cyclosome: A machine designed to destroy. Nat. Rev. Mol. Cell Biol. *7*, 644–656.

28. Lee, L., Tirnauer, J.S., Li, J., Schuyler, S.C., Liu, J.Y., and Pellman, D. (2000). Positioning of the mitotic spindle by a cortical-microtubule capture mechanism. Science *287*, 2260–2262.

29. Korinek, W.S., Copeland, M.J., Chaudhuri, A., and Chant, J. (2000). Molecular linkage underlying microtubule orientation toward cortical sites in yeast. Science *287*, 2257–2259.

30. Miller, R.K., Cheng, S.C., and Rose, M.D. (2000). Bim1p/Yeb1p mediates the Kar9p-dependent cortical attachment of cytoplasmic microtubules. Mol. Biol. Cell *11*, 2949–2959.

31. Moore, J.K., and Miller, R.K. (2007). The cyclin-dependent kinase Cdc28p regulates multiple aspects of Kar9p function in yeast. Mol. Biol. Cell *18*, 1187–1202.

32. Maekawa, H., and Schiebel, E. (2004). Cdk1-Clb4 controls the interaction of astral microtubule plus ends with subdomains of the daughter cell cortex. Genes Dev. *18*, 1709–1724.

33. Ding, D.Q., Yamamoto, A., Haraguchi, T., and Hiraoka, Y. (2004). Dynamics of homologous chromosome pairing during meiotic prophase in fission yeast. Dev. Cell *6*, 329–341.

34. Ding, D.Q., Chikashige, Y., Haraguchi, T., and Hiraoka, Y. (1998). Oscillatory nuclear movement in fission yeast meiotic prophase is driven by astral microtubules, as revealed by continuous observation of chromosomes and microtubules in living cells. J. Cell Sci. *111*, 701–712.